AD/A-004 861

MONOSTATIC MICROWAVE IMAGING OF BURIED OBJECTS. VOLUME I

O. Yue, et al

General Dynamics

Prepared for:

Army Mobility Equipment Research and Development Center

October 1974

UNCLASSIFIED

SECURITY CLASSIFICATION OF THIS PAGE (When Data Entered)

REPORT DOCUMENTATION PAGE		READ INSTRUCTIONS BEFORE COMPLETING FORM
1. REPORT NUMBER	2. GOVT ACCESSION NO.	3. RECIPIENT'S CATALOG NUMBER AD/A-004861
4. TITLE (and Subtitle) Monostatic Microwave Imaging of Buried Objects, Vol. 1.		5. TYPE OF REPORT & PERIOD COVERED Final; March 1974, to Oct. 1974 6. PERFORMING ORG. REPORT NUMBER R-74-96
7. AUTHOR(s) O. Yue, G. Tricoles, E. L. Rope		8. CONTRACT OR GRANT NUMBER(s) DAAK02-71-C-0264
9. PERFORMING ORGANIZATION NAME AND ADDRESS General Dynamics Electronics Division P.O. Box 81127, San Diego, CA. 92138		10. PROGRAM ELEMENT, PROJECT, TASK AREA & WORK UNIT NUMBERS
11. CONTROLLING OFFICE NAME AND ADDRESS U.S. Army Mobility Equipment Research and Development Command Fort Belvoir, VA.		12. REPORT DATE October 1974 13. NUMBER OF PAGES 49
14. MONITORING AGENCY NAME & ADDRESS(if different from Controlling Office) N/A		15. SECURITY CLASS. (of this report) None 15a. DECLASSIFICATION/DOWNGRADING SCHEDULE
16. DISTRIBUTION STATEMENT (of this Report) N/A		
17. DISTRIBUTION STATEMENT (of the abstract entered in Block 20, if different from Report) N/A		
18. SUPPLEMENTARY NOTES N/A		
19. KEY WORDS (Continue on reverse side if necessary and identify by block number) Microwaves Imaging Holography Inverse Scattering		

20. ABSTRACT (Continue on reverse side if necessary and identify by block number)
High quality microwave images of realistic objects in damp soil were formed, and correlated to the structure of the objects using the monostatic measurement technique. Moreover, they compared very well with other images made in dry smooth soil. Effect of polarization and changes in frequency on the microwave image was investigated. A new way of displaying the scanned data was introduced to facilitate detection of buried objects.

DD FORM 1 JAN 73 1473 EDITION OF 1 NOV 65 IS OBSOLETE

UNCLASSIFIED

SECURITY CLASSIFICATION OF THIS PAGE (When Data Entered)

PREFACE AND ACKNOWLEDGEMENT

The work described in this report was performed in association with the Mine Detection Division, Countermine and Counter Intrusion Department of the U. S. Army Mobility Equipment Research and Development Center, Fort Belvoir, Va., under contract DAAK02-71-C-0264. The Project Engineer was D. Hess.

This report consists of two volumes; all confidential information is collected in Volume 2. Part of the data used in this report was gathered at the National Bureau of Standards under the supervision of F. Clague whose cooperation is gratefully appreciated. The authors received guidance, suggestions, and constructive criticisms from A. Leff and D. Hess of USMERDC.

CONTENTS

ILLUSTRATIONS

1. SUMMARY AND RECOMMENDATIONS

High quality microwave images of realistic objects buried in moderately damp (3% to 5%) smooth soil have been produced in this program. The data were taken by NBS (National Bureau of Standards) at their test site. The objects were buried at depths of one to five inches and a scanning antenna was four inches above the soil surface.

This program is part of the continuing effort to apply microwave techniques to detect and identify buried objects. Previous study demonstrated the feasibility of imaging rectangular boxes in smooth dry soil [1] and developed image processing techniques that were used in this program. The quality of the images produced from the NBS data was verified by additional microwave images of the same objects made under ideal laboratory conditions at Electronics Division. A new method to display the unprocessed data was also studied and found to be a valuable tool for preliminary detection of buried objects.

The microwave imaging system that has been studied in this program has two important features. It produces visual images that a human operator can interpret, and the necessary components are commercially available equipments. The results to date have been very promising, and it is recommended that this technique be studied further, specifically in the following areas:

---

[1] As reported in Reference 1.

1) Surface Reflection Estimation

It has been shown irrefutably that subtraction of the front surface reflection enhances the image quality as well as the probability of detection tremondously. Better surface fitting algorithms should be developed for this purpose; in addition, wave polarization should be exploited to reduce the random variation in the reflected component. Profiling the surface with an independent source should be investigated, accompanied by analytical work in rough surface scattering, relating the received component at the antenna to the actual surface. The latter may be avoided if it can be shown that other waves with comparable wavelength in air have a similar kind of reflection property from the soil as microwave but negligible penetration depth. High frequency microwaves or acoustic waves might be used. Light waves might be useful but scattering by a rough surface may require special techniques such as a mosaic of detectors. This imaging technique should also be tested for rougher surfaces.

2) Microwave Image Signature

Three objects were investigated in this program at various depths and frequencies. Additional images should be formed with other combinations of depth and frequency to learn more about the characteristics of the microwave images of different objects, including other objects of interest besides the ones considered. This information would be used for identification and to reduce the probability of false alarm and misses. Wave polarization is another parameter that could be varied to enhance edges in

images. The influence of the antenna coverage should be considered and compared to the size of the reflecting region of the object.

3) Rapid Data Acquisition

A single antenna can be scanned over an area, but the motion retards data acquisition. The data flow can be accelerated by an array of switched antennas. Switching greatly reduces energy transfer between antennas because only mutual coupling between the active element and its passive neighbors occurs. Of course, antenna spacing should be small enough to avoid missing the objects.

4) Preliminary Detection

The use of reflection vector locus (RVL) plots have been introduced and should be investigated further for detections. RVL plots of other objects should be obtained so that their patterns can be recognized.

5) Integrated Detection System

An interactive computer program has been written on a 16-bit machine with 64K memory to form the images. One minicomputer can handle both the data acquisition controls and the calculations. A dedicated system should be built and field tested.

2. MEASUREMENT AND PROCESSING TECHNIQUES

The data gathering procedure and the image forming algorithm used in this program are identical to those developed in the previous program [1]. In this section we shall describe these techniques briefly. For more details the readers are referred to Reference 1.

The monostatic measuring technique was used throughout this program to synthesize holograms for processing. The principal equipments are a single antenna which both transmits and receives, a reflection transmission test unit, a network analyzer and a recording device (Figure 2-1). The antenna was a pyramidal horn with E-plane dimension 8.6 cm and H-plane dimension 10.9 cm.

Data is collected by scanning the antenna at a fixed height (4 in) above the soil surface and sampling the amplitude and phase at equal spacings (1 in). After moving the antenna the same interval of 1 inch in the cross-track direction, the antenna is scanned again. This procedure is repeated until an area that will more than cover the buried object has been sampled. In most cases the E-plane of the horn is parallel to the scanning direction which is vertical in all images (we refer to the data as the E-plane cuts), but we have also changed polarization to study its effect. The antenna was tuned to a VSWR of less than 1.02 in free space and the accuracy of the amplitude and phase was $\pm$ 0.5 dB and $\pm$ 5 degrees respectively.

[1] G. Tricoles, E. L. Rope, O. C. Yue, General Dynamics Report R-73-039, July 1973, Final Report for Contract DAAK02-71-C-0264.

After the holograms have been synthesized, the data is entered into a computer and the images are computed in two steps. First, the background noise is estimated and subtracted, then the wavefront at the object is reconstructed using the angular spectrum method.

In a first order, approximate model of the signal return, the reflected field consists of the object scattered field (signal) and the reflection at the air-to-soil interface (noise). The latter can be a constant for smooth surfaces or completely random over the hologram for rough surfaces. In addition the hologram plane may not be parallel to the average soil surface, resulting in nonstationarity of the noise.

In this program we have restricted our investigation to noises which have small variances but nonstationary means, so that we can approximate the noise with a single tilted plane or a composite surface consisting of several locally planar surfaces at different slopes. Since the noise is a complex-valued quantity, two surfaces have to be estimated for either the real and imaginary parts or the magnitude and phase. For small noise variances both combinations yield almost identical results and the former was used throughout this program to reduce computation time.

After the estimated noise distribution has been subtracted from the data, the wavefront at the hologram plane of the wavefront is backward propagated to the object plane, using the angular spectrum diffraction model. The

monostatic method of data acquisition causes the wavelength used in the computation to be halved, otherwise the propagator is identical to that for the conventional microwave holographic system. Since the wave travels through two media with different dielectric constants, the wavelength should be modified accordingly for propagation in the soil. However, just like the human eye uses the same "algorithm" to image an object submerged in water as well as in free space, the subtracted holograms were backward propagated directly across the air-to-soil interface without changing wavelength. By the same analogy the imaging distance would be different from the true depth, so the image forming algorithm has a propagation distance parameter that can be adjusted to bring the image into focus.

Elimination of changing wavelength in the soil is a very important feature of our imaging system. The reason is that the dielectric constant of the soil is an unknown varying with soil type and moisture content, and in general it is not feasible to measure it. Moreover, in a practical system the imaging distance has to be adjusted to search for an object of unknown depth anyway. One noticeable effect of not changing wavelength is that the size of the image is smaller than that of the object but having the same shape, like the visual image of a submerged object again. This effect is more pronounced for deeper objects, wetter soil conditions, and higher frequency.

The entire imaging algorithm requires an operator to control two parameters. The background noise estimates have to adjust to obtain the cleanest possible

subtracted hologram, and the propagation distance has to be adjusted. Therefore, an interactive imaging program has been implemented on a 16-bit word minicomputer with 64K memory and a CRT terminal. Even with this relatively slow processor, an operator can see the effect of the inputted modification on the image within minutes. Two methods of displaying the intensity distribution were used: fixed size squares of different gray levels and variable size solid black squares. High intensity regions are shown as white or almost blank patches.

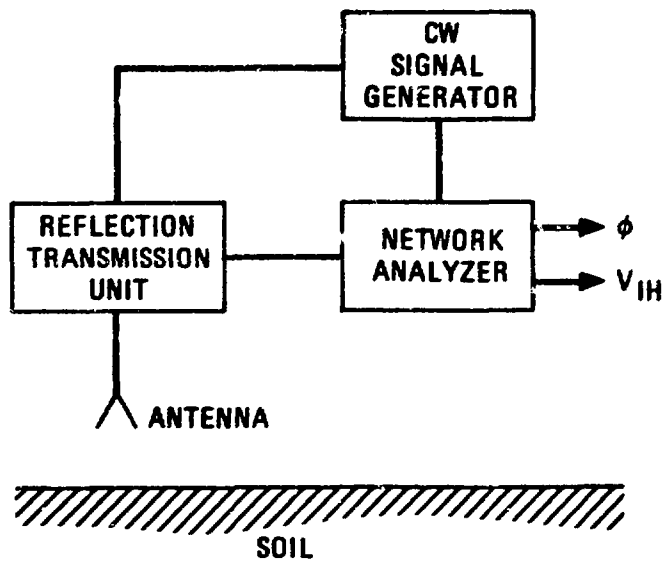

Figure 2-1. Monostatic Measurement Apparatus.

3. DESCRIPTIONS OF OBJECTS AND THEIR MICROWAVE IMAGES

Three different types of objects were studied in this program. Data were taken initially at the National Bureau of Standards (NBS) where the test site was divided into six sectors (I to VI), and two type-A, one type-B, and three type-C were buried at various depths, as described in Table 1. Additional data on objects types B and C was gathered at General Dynamics/Electronics Division (GD/E) under similar but more controlled conditions: dry soil and smooth surface. The purpose of the latter was to produce microwave image standards that can be used as basis for determining image quality. In the first-order model developed in the previous program multiple reflections are omitted so that the measured signal consists of reflections due to all dielectric discontinuities. In this section we shall correlate the image standards to the structure of the objects.

Since the soil surface was carefully smoothed, the reflection by the air-to-soil interface was constant throughout the hologram. This component was measured by placing the antenna far enough away from areas where the objects were buried, and then subtracted from the hologram.

All images shown in this section were made at αHz (see Table 1 in Vol. 2 for frequency assignments) from data measured at GD/E. Each one has a dynamic range of 15 dB and the intensity is displayed logarithmically by 8 gray levels which are indicated by solid black squares of different sizes with white corresponding to the maximum. The field of view in every case is 32 in. x 32 in., covered by 64 x 64 resolution cells.

Object A has a rectangular void of uniform thickness. Microwave images of this type of object were produced in the previous program, showing rectangular concentration of energy as expected. So image standards for object A were not necessary. The size of the void was 9.5 in. x 11.5 in. x 1 in.

The mechanical drawing of object B in Figure 1 of Vol. 2 shows a circular void of radius 2.5 in. in the middle but the thickness varies from 0.3 in. to 1.2 in. The housing material is white and feels like hard paraffin. Figure 3-1 is an image of object B in Sector III; it has a circular bright spot of about 2.0 in. radius. The finer details of the void are much smaller than the wavelength radiated so they are not discernible in the image. Since other parts of the object did not reflect any energy, it can be concluded that there are no other dielectric discontinuities inside. Moreover, it is surmised that structural material of object B has a dielectric coefficient very close to that of the soil.

The mechanical drawing of object C in Figure 2 of Vol. 2 shows several annular voids with a circular one in the center. However, their thickness and location in depth are different, and depending on the illuminating frequency they may appear distinctly or smeared out. One possible grouping of these voids is according to depth. The deeper ones constitute a cylinder, 4.5 in. diameter and 1 in. deep, but the others group into a single annulus with inner and outer diameters of 5 in. and 10 in. respectively. The case is plastic, about 0.2 in. thick and has dimensions 12.5 in. x 12.5 in. x 2.5 in. Two

images of object C are shown in Figure 3-2, corresponding to Sectors IV and V and there is a 4 in. diameter circle in the middle of both. In Figure 3-2a there are two elongated vertical bright spots with outside dimensions of 11 in. on both sides of the circle, enclosing it like a pair of parentheses. In the upper right hand portion of the image a 90 degree corner is also discernible. In Figure 3-2b in addition to the pair of highlighted parentheses, the lower intensity levels almost trace out a 11 in. x 11 in. polarization square with very sharp corners. The rectangular shape indicates that there are other dielectric discontinuities present beside the circular voids. From their relative densities, it is reasonable to assume that the dielectric constant of the plastic case exceeds that of the filler, which is approximately the same as that of the soil. So the case acts like a resonant cavity and reflects a strong return.

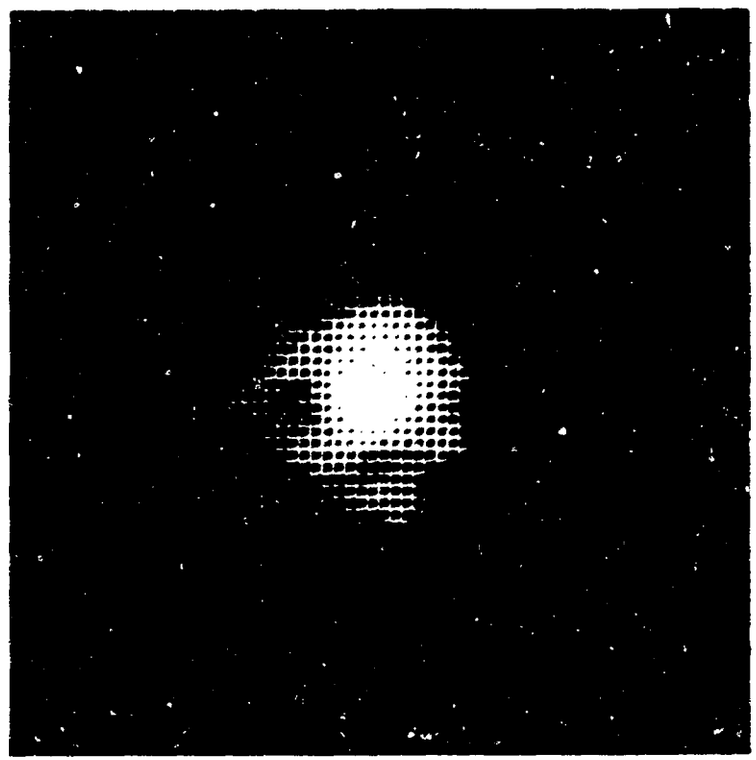

Figure 3-1. Image of Object B in III at α Hz

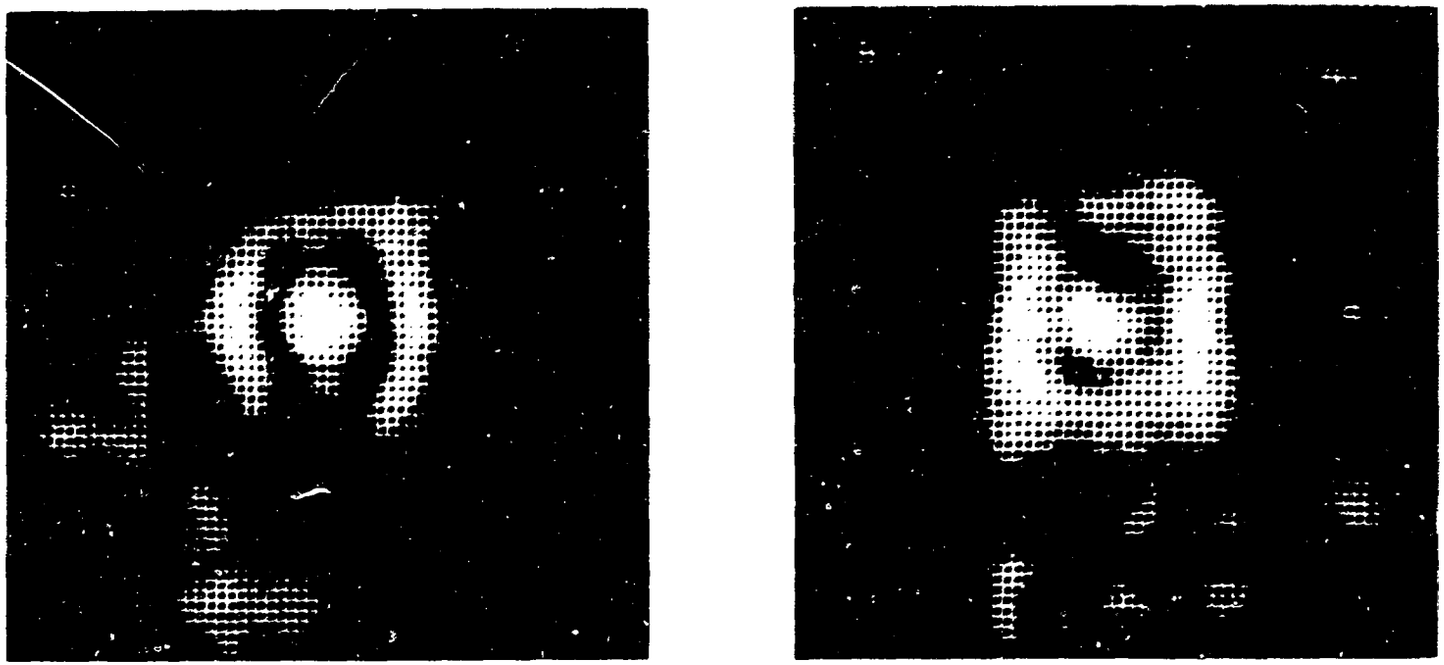

a) Sector IV

b) Sector V

Figure 3-2. Images of Object C in IV and V at α Hz

4. IMAGES OF OBJECTS BURIED IN DAMP SOIL

Two sets of data were collected by NBS personnel at their test site as described earlier. The frequency used in the first set was αHz. The water content of the soil was sampled and found to vary between 5% and 6% by weight; the saturation level is about 15%. In the second set βHz was the frequency, and it is estimated that soil has dried to about 3% moisture content. The test plot was 80 in. by 120 in. and with the moderately damp soil the smoothest surface obtainable still has slight undulations with crest-to-trough heights of about 1 in. in some sectors. In this section we shall present some subtracted holograms and images from all sectors at both frequencies.

Subtracted holograms are obtained by subtracting the estimated noise component from the original sets of data vectorially. The sampling intervals in both directions are 1 in. so each sector was covered by a 40 x 40 complex matrix. Since the data were taken 4 in. above the surface, the object-scattered field has diffracted negligbly, and knowing the exact location of the object we can isolate the region of the hologram that contains significant information to a 16 in. x 16 in. area. The rest can be attributed entirely to reflection by the soil surface and provides information for estimating the noise component over the object. To illustrate the behavior of the noise, some typical scans over these signal-free regions are plotted in the complex plane in Figures 4-1 and 4-2; these are the loci of the tip of the signal

reflection vector. Notice how the loci in Figure 4-1 cluster around a single point, representing scans over smooth surfaces. In contrast Figure 4-2 shows examples of rough cases; the differences are self-evident. With this kind of nonstationarity in the noise, a multi-faceted surface is necessary to estimate the varying surface reflection component in the hologram.

The size of the hologram at each sector is reduced to 32 x 32 to take advantage of a radix-2 FFT subroutine. Then the matrix is divided into quadrants, and using the data in the signal-free regions planes are fitted in each quadrant for the surface reflection and subtracted from the hologram. The effect of this kind of subtraction can be seen in Figures 4-3 and 4-4, which show the original and subtracted holograms of Sectors I and IV taken at βHz. One striking difference between the holograms in both figures is the almost complete reversal of tone from one to the other. The reason is that while the subtracted hologram displays the diffraction intensity which goes to zero (black) as the distance from the object increases, the original hologram is basically an interference pattern which shows nulls (black) only when the object scattered and the surface reflected fields are out of phase. It is interesting to observe that the presence of object C is readily discernible from Figure 4-4a, but the original hologram of object A gives no indication of a buried object. So although the original holograms can sometimes allow detection directly, they are not as reliable as the processed ones.

The surface fitting algorithm used is a very simple one for planes and allows the operator to adjust one complex parameter for better noise suppression in the region directly above the object. There are better and more complicated surface fitting algorithms but they would require either independently acquired data about the surface, at a higher frequency for example, or knowledge about the behavior of the surface reflection that distinguishes itself from the object scattered field. This is one of the areas where more investigations would be very fruitful in producing better images.

The images at the different sectors are shown in Figures 4-5 through 4-10, each one displaying the results for the two frequencies. The intensity is displayed logarithmically by 10 gray levels covering a dynamic range of 15 dB. The field of view is 32 in. x 32 in. with 64 x 64 resolution cells. The images of object A in Figure 4-5 clearly indicates the rectangular shape and since the depth is shallow the size corresponds to the object dimensions very well. In Sector II the image at αHz still shows a rectangular shape but the right half of object A gave a much stronger return than the other half. Similarly at βHz Figure 4-6b shows a rectangular outline despite the noisy background. Comparing Figures 4-5 and 4-6 the deterioration in image quality is surprising considering the small change in depth from Sector I to II. We surmise that the major cause for the degradation was the roughness in Sector II. It is interesting to compare Figures 4-3a, 4-3b and 4-5b in sequence, since they illustrate the results from the different stages of processing. Each one was an improvement over the previous one for while the subtracted hologram indicates a rectangular shape, it takes the reconstructed image to bring the object into focus.

Figure 3-1 demonstrated that object B has a small scattering cross-section in the soil, with none of the finer details of the void discernible. However, the image in Figure 4-7a shows a bright spot in the middle with a circular ring around it, while the one at βHz is almost a completely solid disk like Figure 3-1. The difference between the three images of object B may be attributable to variations in frequency and soil condition. The small scattering cross-section makes it difficult to identify and additional images of object B should be made with different soil conditions, frequencies and object depth to learn more about the behavior of its microwave image. However, considering the shape of the void in object B, we do not expect any other kind of variation in the image besides the one that has already been observed in this program: from solid circles to rings around a center bright spot.

Object C was buried at three different depths and there is quite a bit of variation in the resulting images. At αHz the image in Figure 4-8a shows a bright spot in the middle enclosed by a square boundary which is about 12 in. on the side. In Figure 4-9a a long vertical strip with two short horizontal bars on the right are visible. If there were another strip to the right of the bars, the square outline would be complete. One striking difference between Figures 4-8a and 4-9a is the missing bright spot in the latter, which could be due to destructive interference in the middle (compare with Figure 5-2b in Section 5). The image of Sector VI at αHz was very noisy. Using the bright spot in the middle of Figure 4-10a as a reference, there are two other strong returns to the upper and lower left of center, which probably correspond

to the two corners of object C. The object scattered field from Sector VI was evidently very weak due to the attenuation of the damp soil, making it very difficult to detect and identify.

The images of object C at βHz are smaller than those at αHz because of the higher frequency. Figure 4-8b looks like Figure 3-2a turned on its side. The image of Sector V shows almost a complete square with a bright spot in the middle. This compares very well with Figure 3-2b which also indicates a strong return from the case of object C. The image of Sector VI is noisy like that at αHz, but a bright spot enclosed by a square is discernible and certainly reveals the presence of an object. Comparing the images of object C at the two frequencies, it can be concluded that the set of βHz is of high quality, especially in Sector V which may be attributable to a right combination of object depth, frequency and soil moisture content.

The images in this section clearly demonstrate the feasibility of identifying realistic objects buried in damp soil. Object C shows up very well at different depths and frequencies. Only one depth for object B was considered and its small scattering cross-section makes it more difficult to identify. However, as more information is gathered about the microwave images of object B and C by varying depth and frequency, identificat would become more reliable.

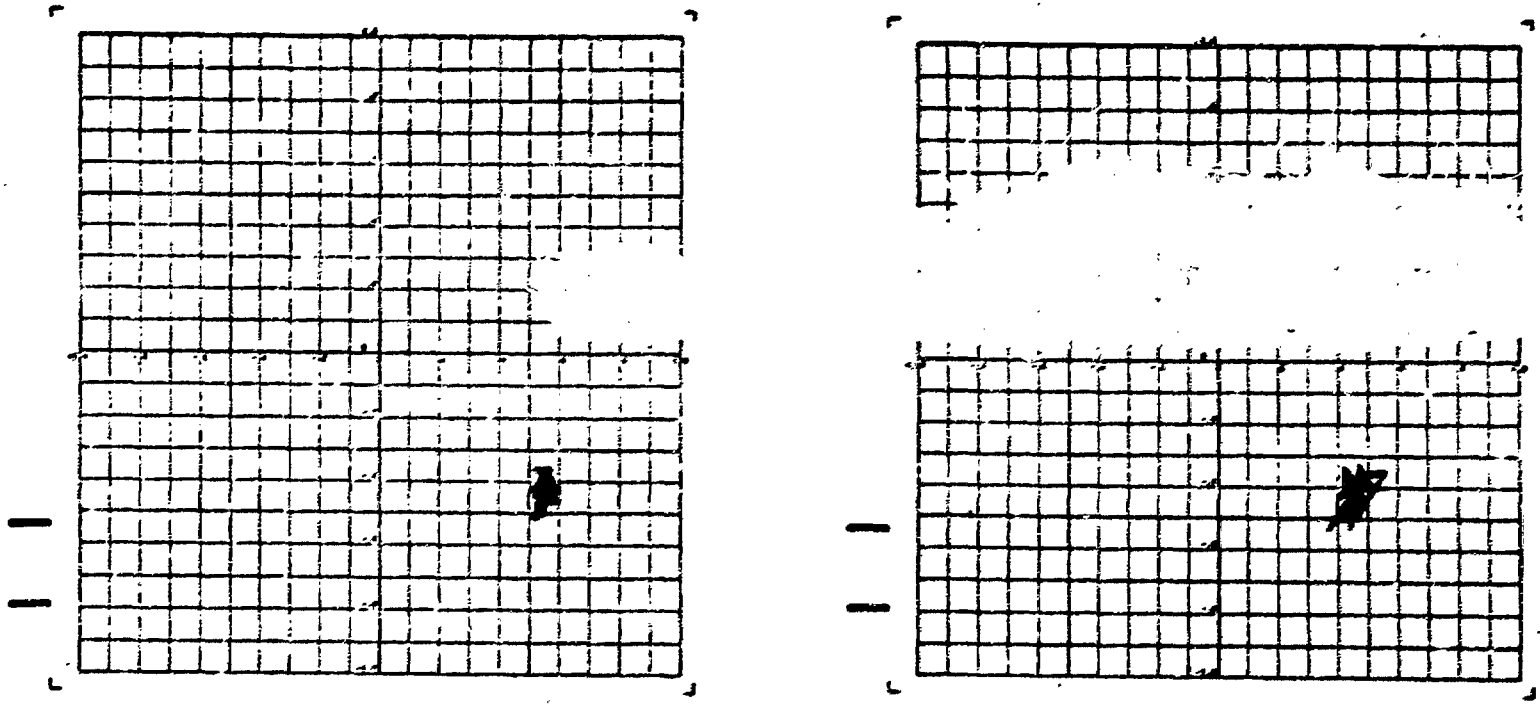

Figure 4-1. Reflection Vector Loci of Smooth Surfaces.

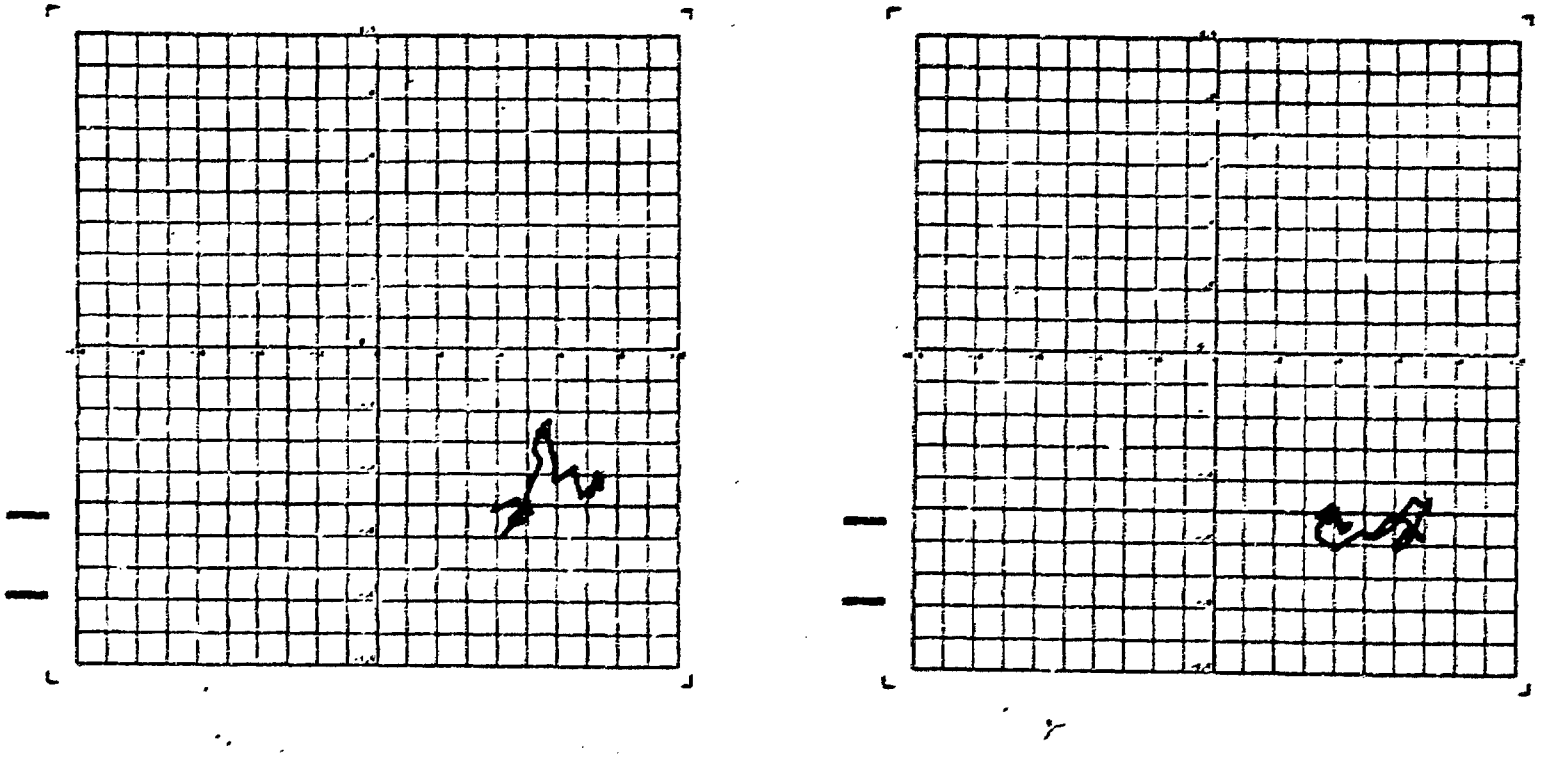

Figure 4-2. Reflection Vector Loci of Rough Surfaces.

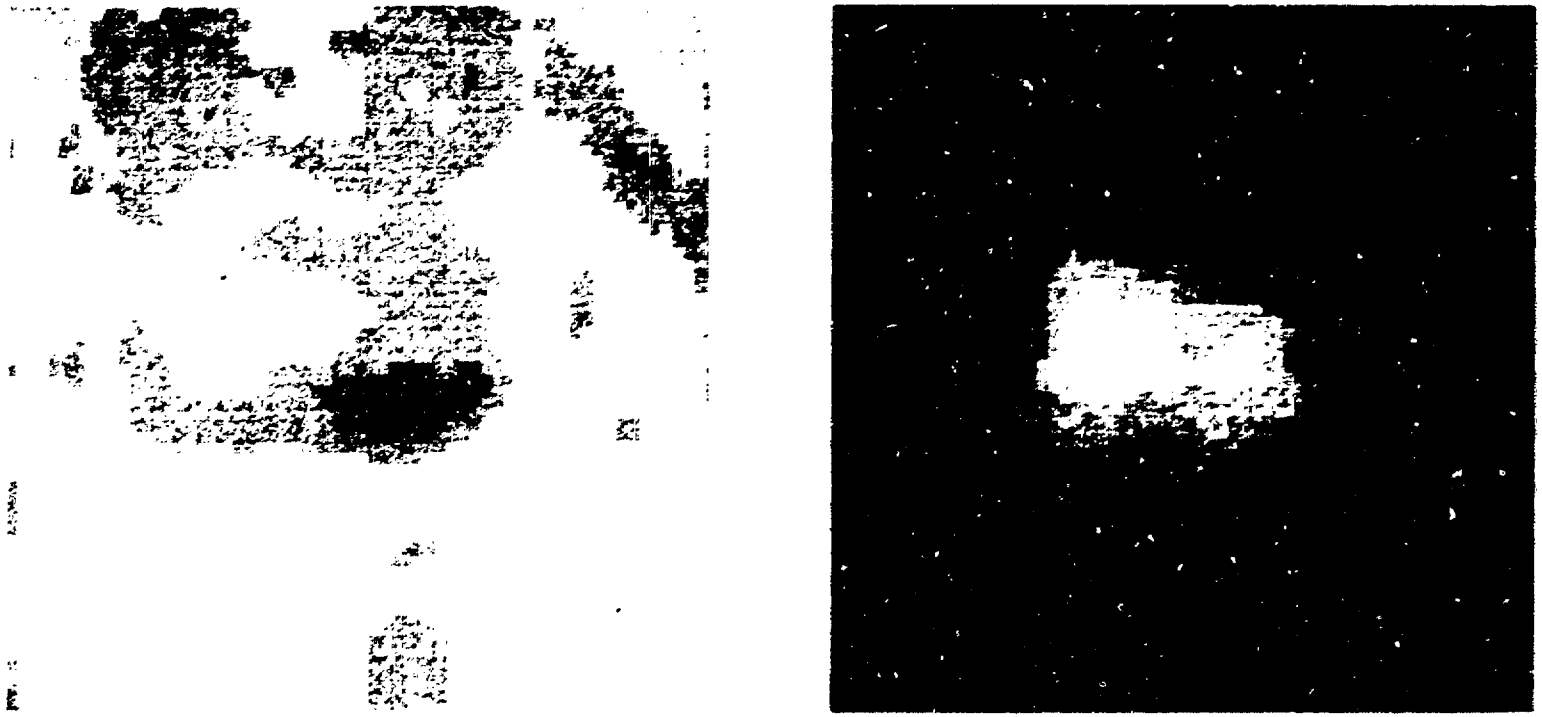

a) Original

b) Subtracted

Figure 4-3. Original and Subtracted Holograms of I at β Hz (NBS)

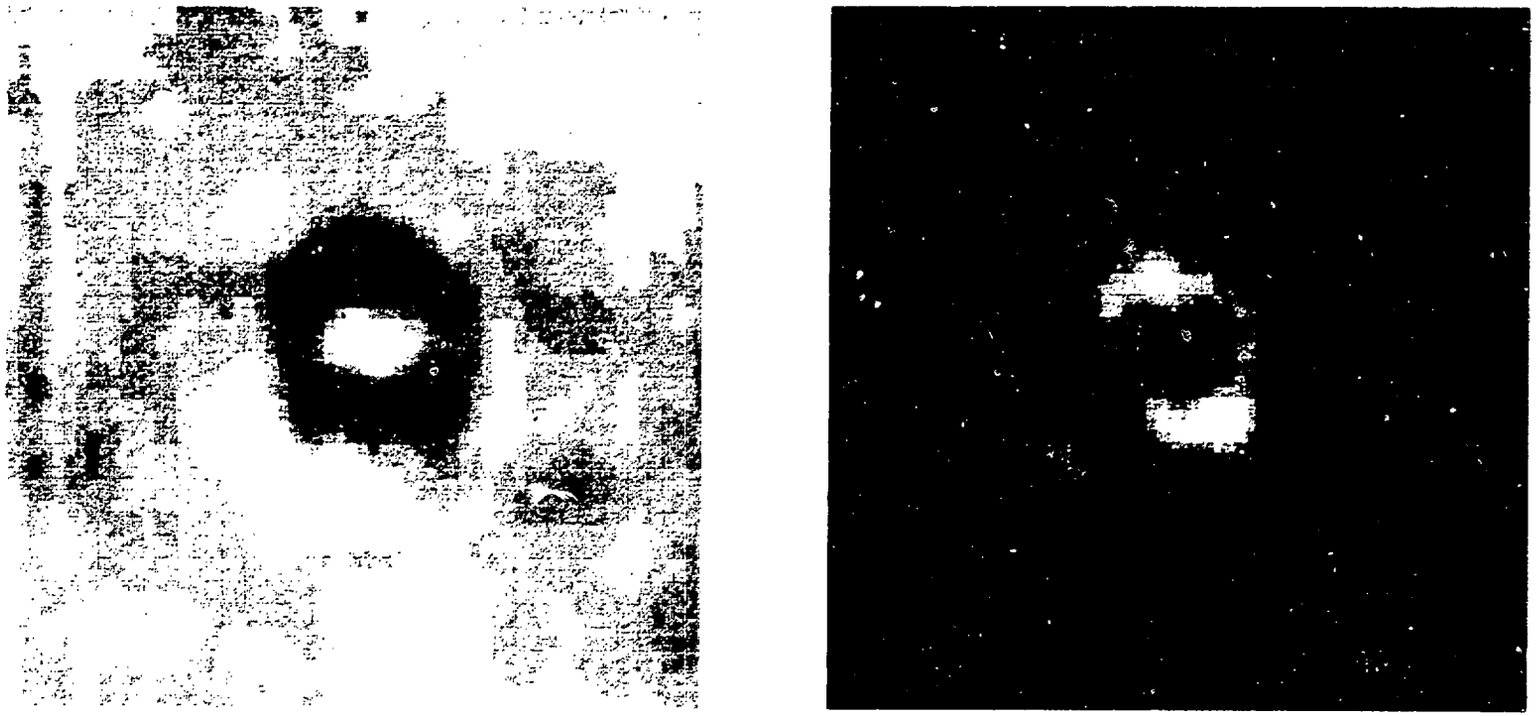

a) Original

b) Subtracted

Figure 4-4. Original and Subtracted Holograms of IV at β Hz (NBS)

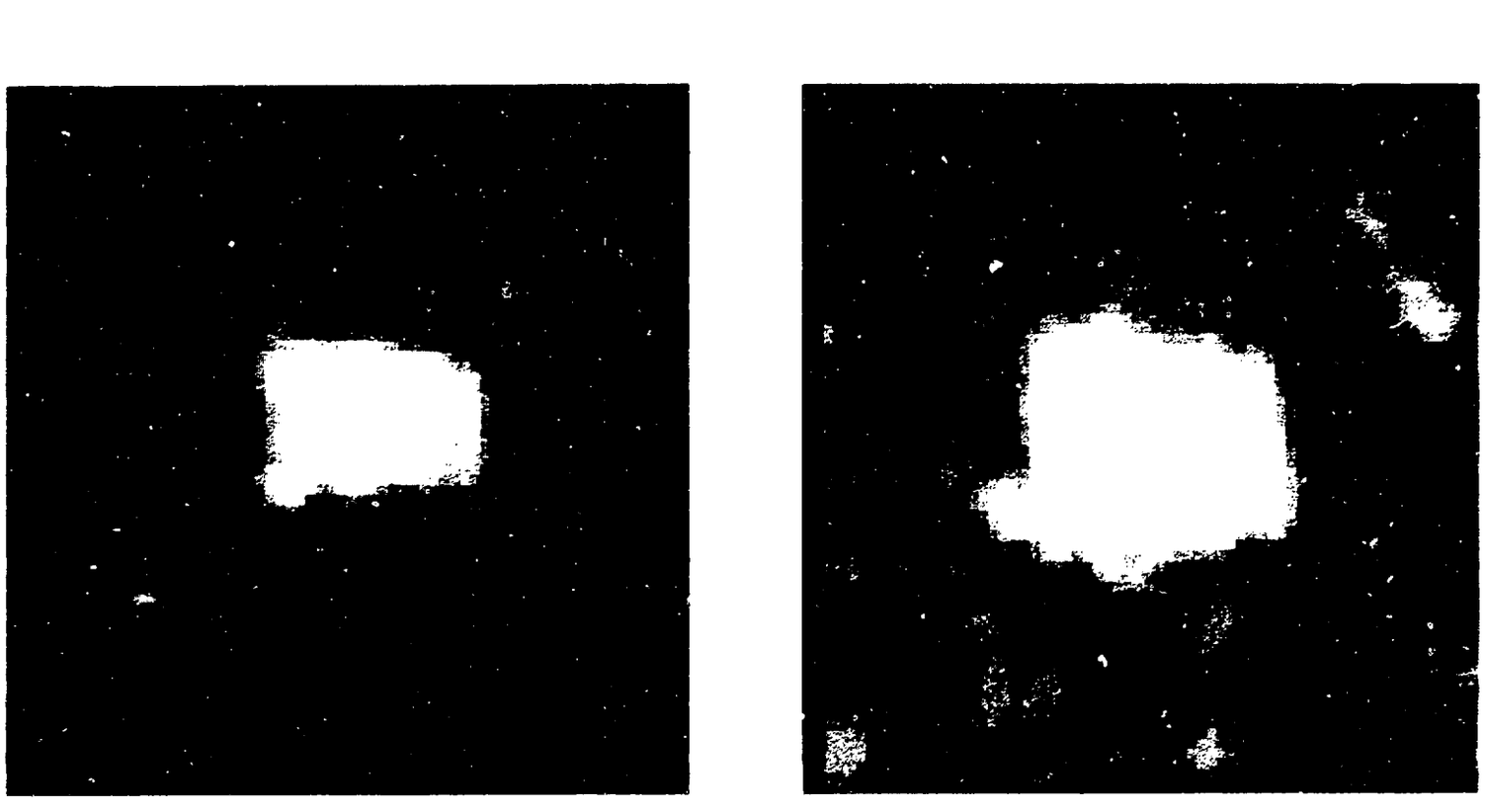

a) α Hz

b) β Hz

Figure 4-5. Images of Object A in I (NBS)

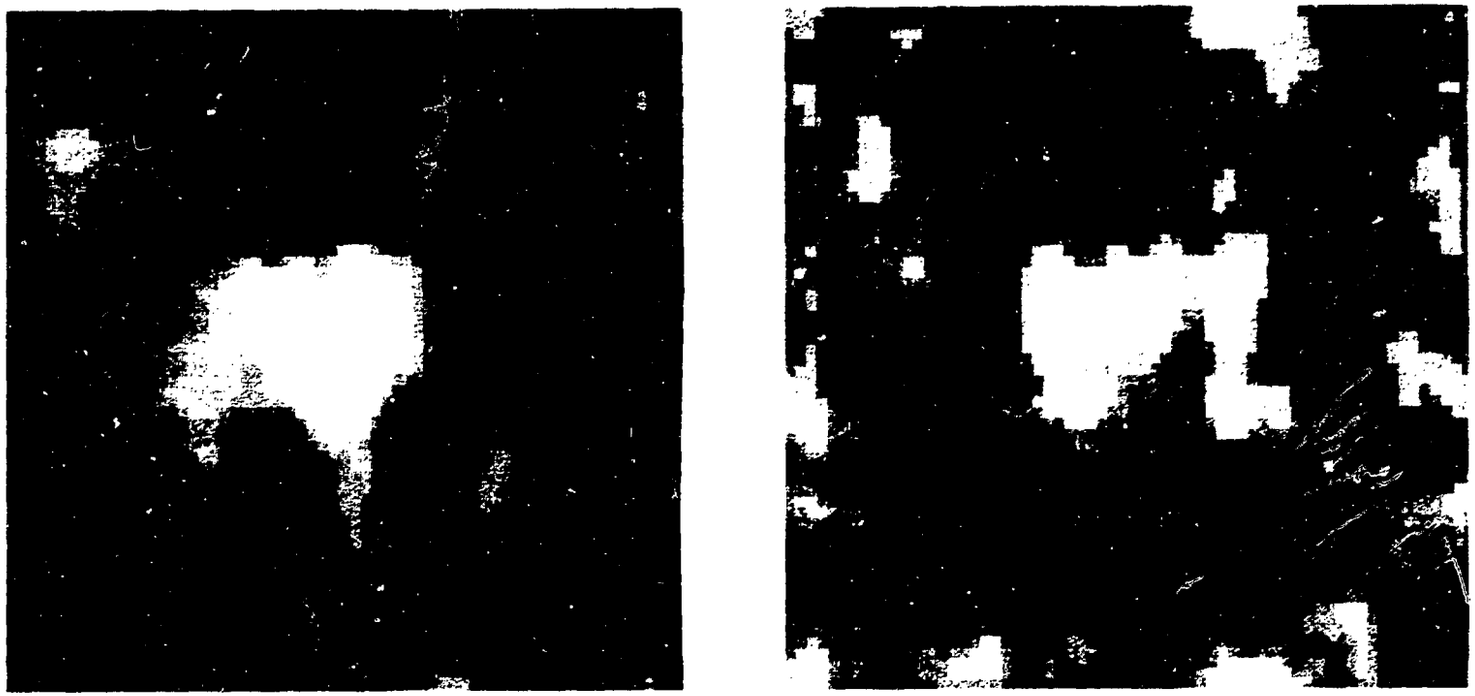

a) α Hz

b) β Hz

Figure 4-6. Images of Object A in II (NBS)

a) α Hz

b) β Hz

Figure 4-7. Images of Object B in III (NBS)

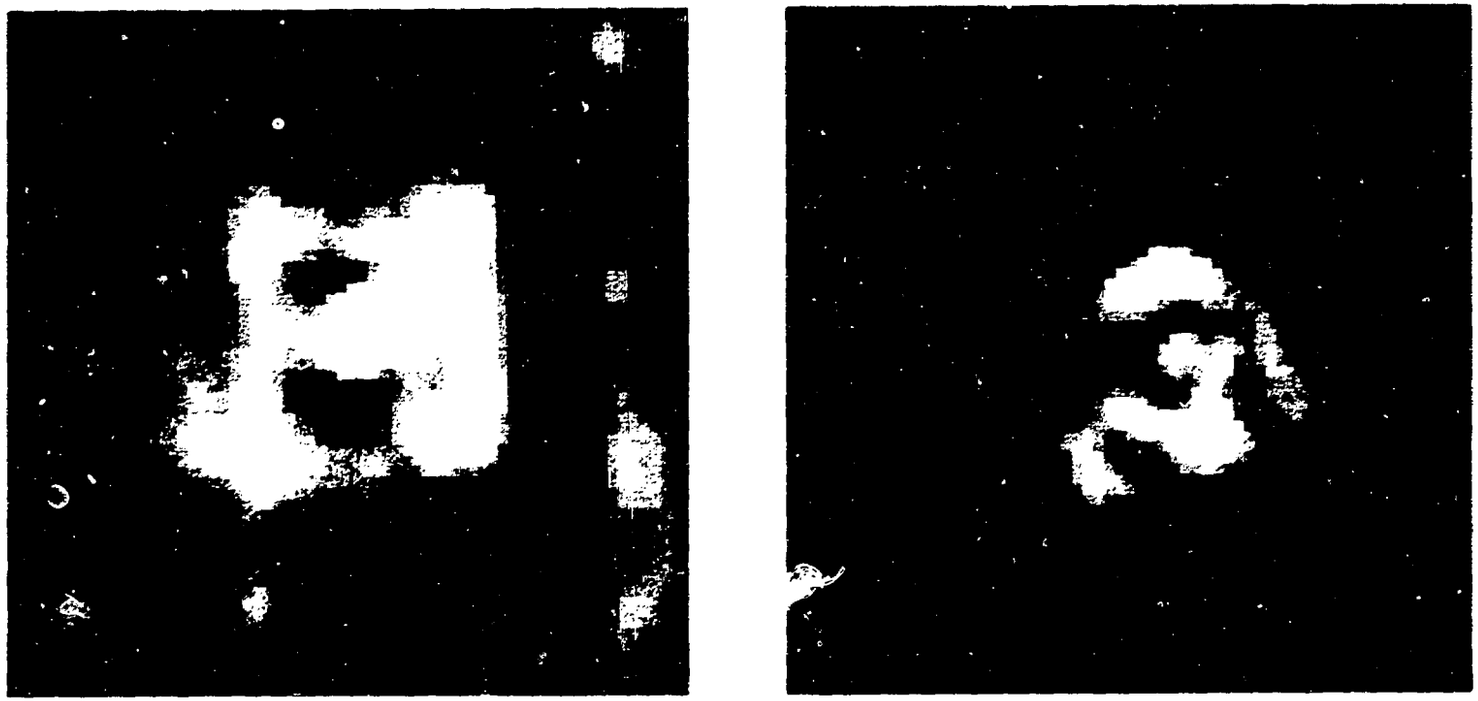

a) α Hz

b) β Hz

Figure 4-8. Images of Object C in IV (NBS)

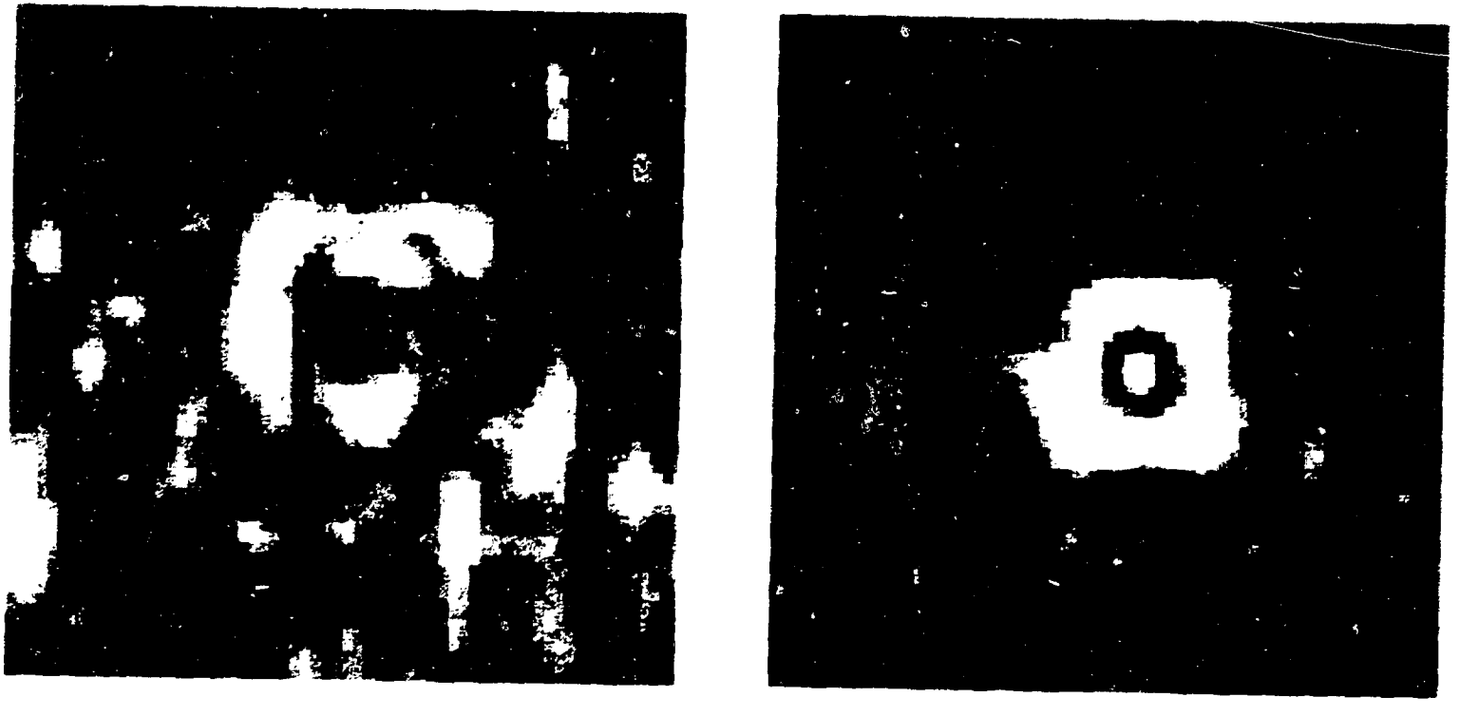

a) α Hz

b) β Hz

Figure 4-9. Images of Object C in V (NBS)

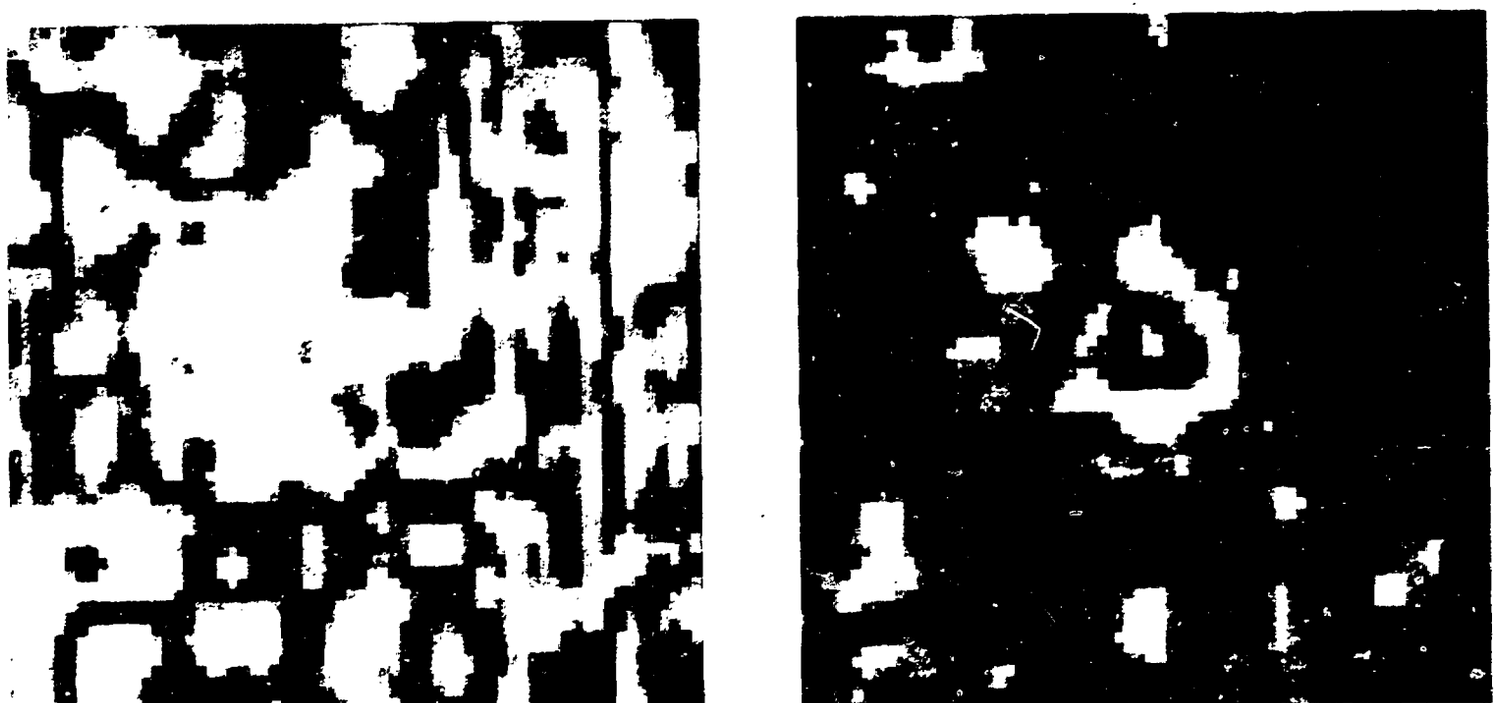

a) α Hz

b) β Hz

Figure 4-10. Images of Object C in VI (NBS)

5. IMAGES AT DIFFERENT FREQUENCIES AND POLARIZATION

Since the choice of frequency is an important design factor in any imaging system, it is of interest to know how the image of an object changes with frequency. Moreover object orientation is always an unknown and so it is also important to study the effect of polarization on the image. Some preliminary investigations have been done in these directions and the results are shown in this section.

The frequency was increased to γHz (see Table I in Vol. 2) and images of objects B and C in conditions of Sector III and IV respectively were made at our laboratory. They are shown along side with the images at αHz in Figures 5-1 and 5-2. The image of object B at γHz is bigger but not substantially different from the one at αHz. On the other hand finer structures in object C are evident in the image at γHz. This confirms our conclusions in Section 3 about the complicated scattering mechanisms in object C. Some of the dark regions in the image, especially in the center, may be due to destructive interference from different parts of the object. There will be some trade-offs in the choice of frequency. Higher frequency would reveal more details of the object, making the identification problem easier, but the shorter wavelength does not penetrate the soil as well and makes the surface "look" rougher, complicating the detection problem. More study is required to decide on the optimum frequency.

All the images shown up to this point were from E-plane cut data, i. e., the E vector is always parallel to the scan direction which is vertical in all figures. It is well-known that the reflection coefficient of any surface is dependent on the polarization of the incidence wave *. So with objects B and C in conditions of Sector III and IV we repeated the experiment at αHz and γHz but obtain H-plane cuts. The resulting images are shown in Figures 5-3 through 5-6 along with the E-plane results. The effect of polarization on the images of object B is insignificant as can be seen in Figures 5-3 and 5-4. This may be attributable to the small scattering cross-section of the object. One noticeable difference between the H-plane and E-plane results in Figures 5-5 and 5-6 of object C is the orientation of the elongated highlights in the image; they are always parallel to the E vector. In fact, if the two images in Figure 5-5 were superimposed, a uniformly bright rectangular ring would emerge. Clearly this suggests acquiring two sets of data with orthogonal polarizations for each situation to increase the probability of identification. Moreover, the soil surface reflection is also sensitive to polarization when it is not perfectly smooth, so orthogonal polarizations may reduce the noise by averaging and improve detectability. The use of circular polarization is another possibility and more study in this area is recommended.

•

* Except for the special case of normal incidence on flat surfaces.

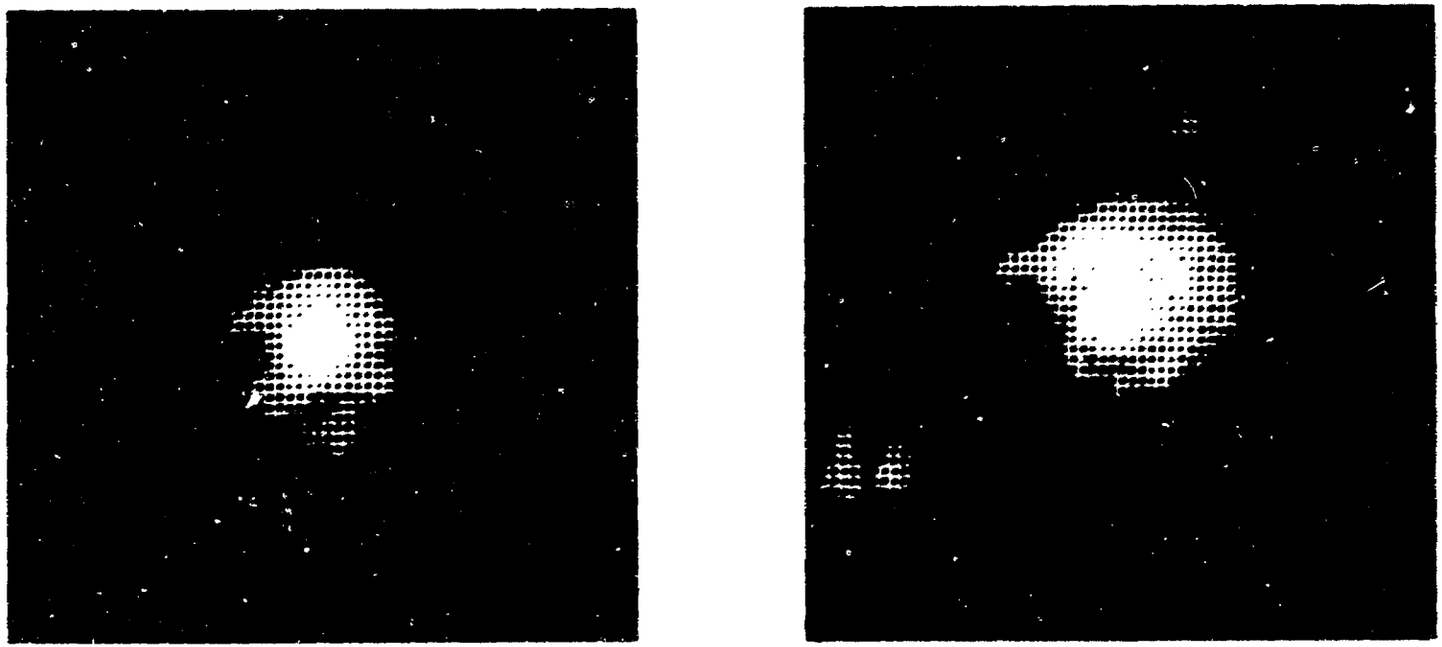

a) α Hz

b) γ Hz

Figure 5-1. Images of Object B in III at α Hz and γ Hz

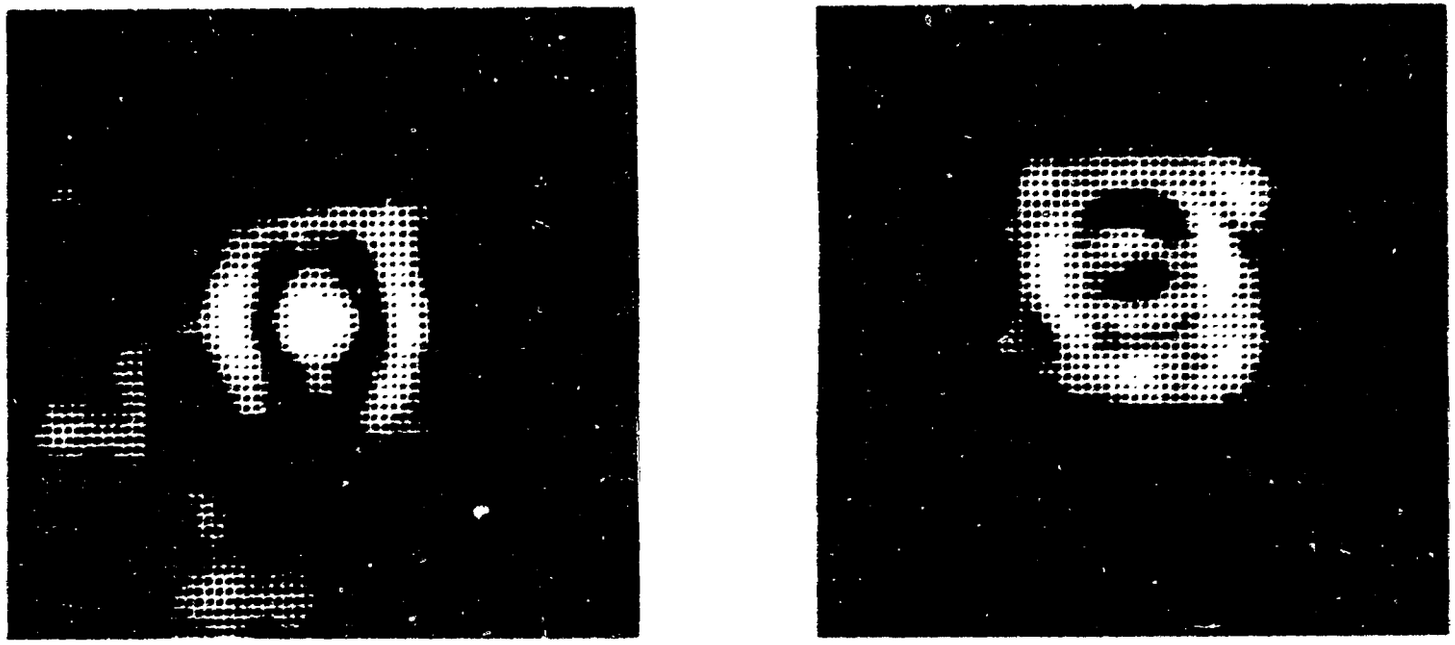

a) α Hz

b) γ Hz

Figure 5-2. Images of Object C in IV at α Hz and γ Hz

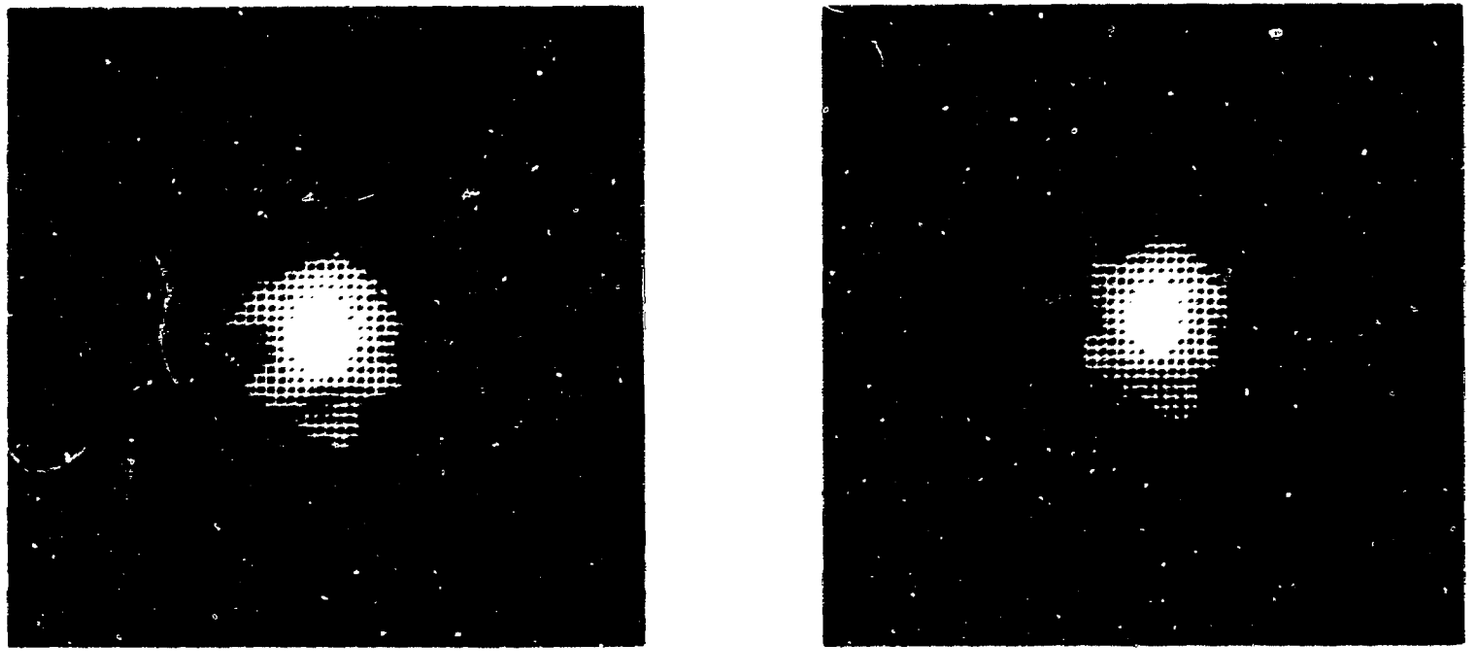

a) E-polarized

b) H-polarized

Figure 5-3. Images of Object B in III with two Polarizations at α Hz

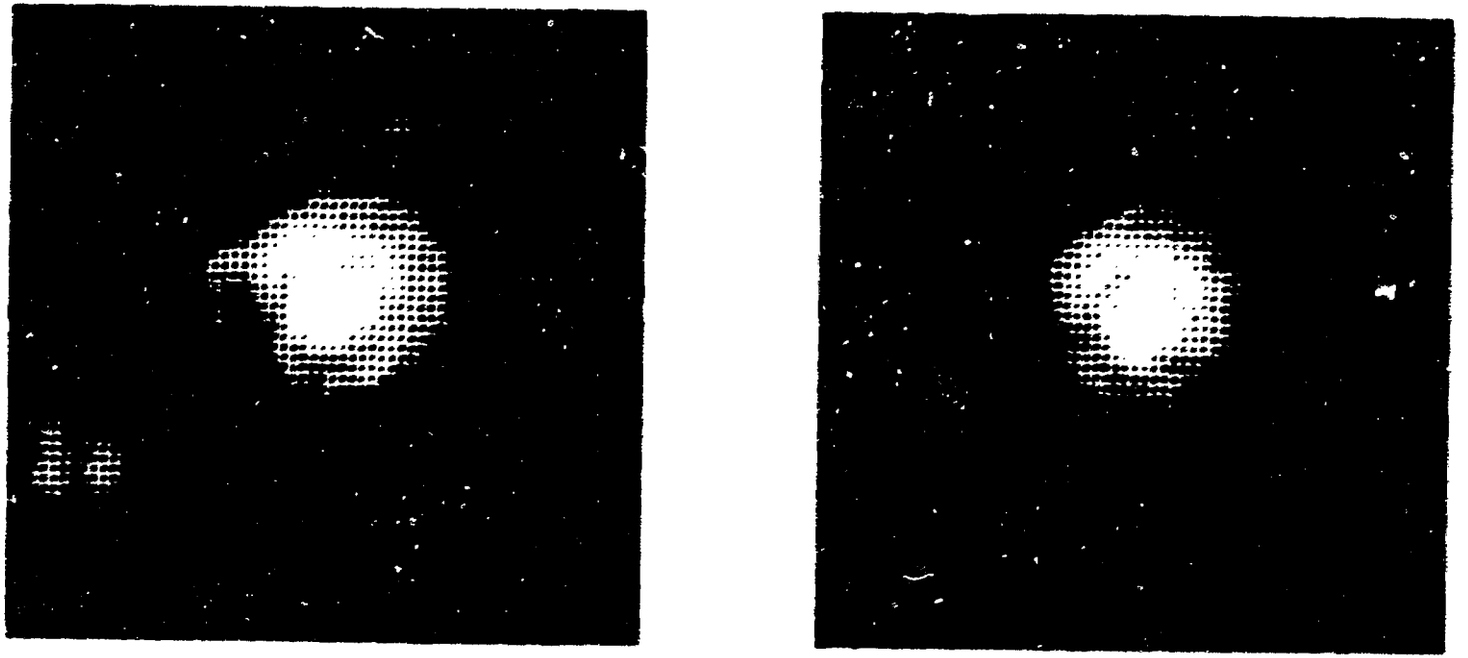

a) E-polarized

b) H-polarized

Figure 5–4. Images of Object B in III with two Polarizations at γ Hz

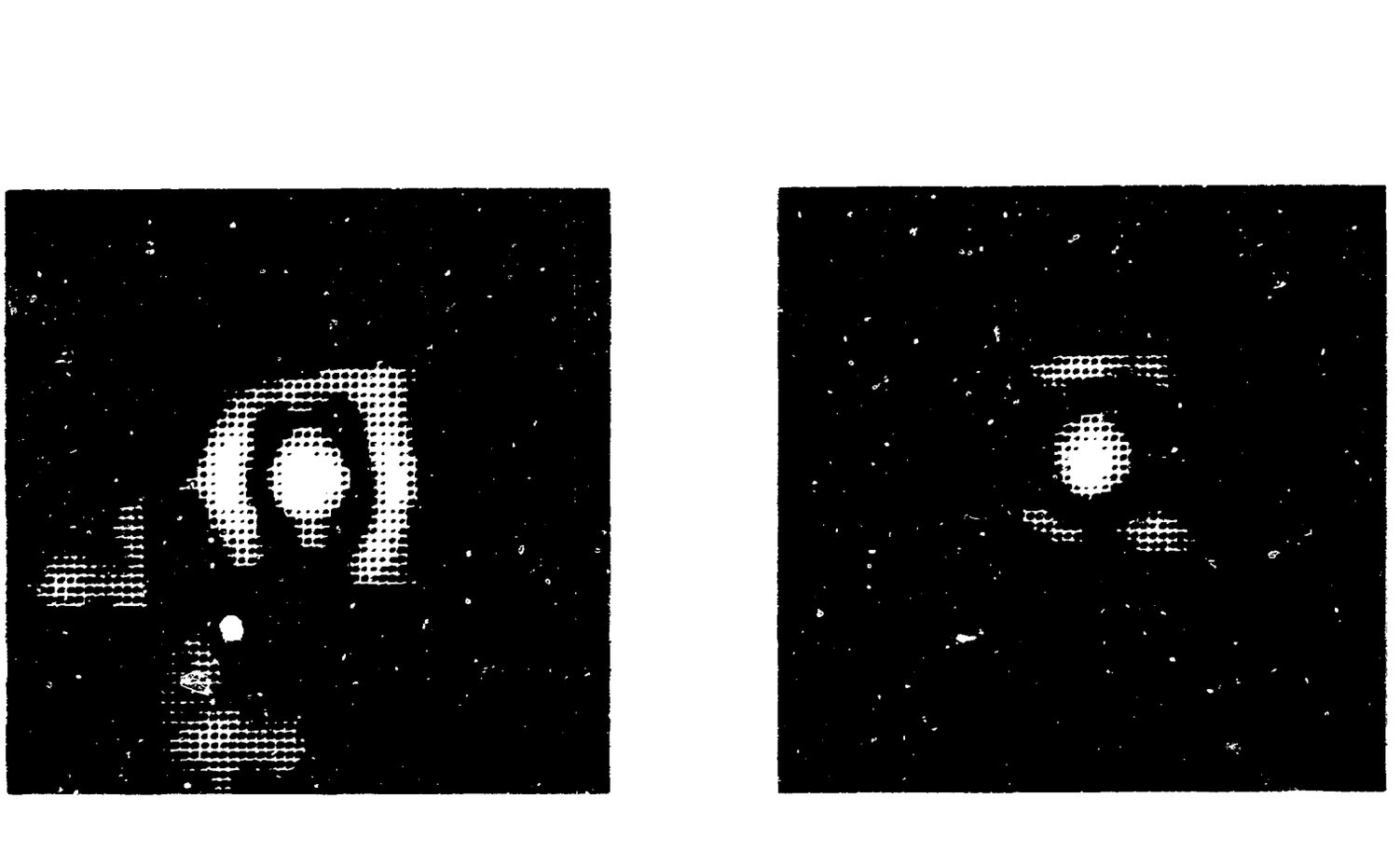

a) E-polarized

b) H-polarized

Figure 5-5. Images of Object C in IV with two Polarizations at α Hz

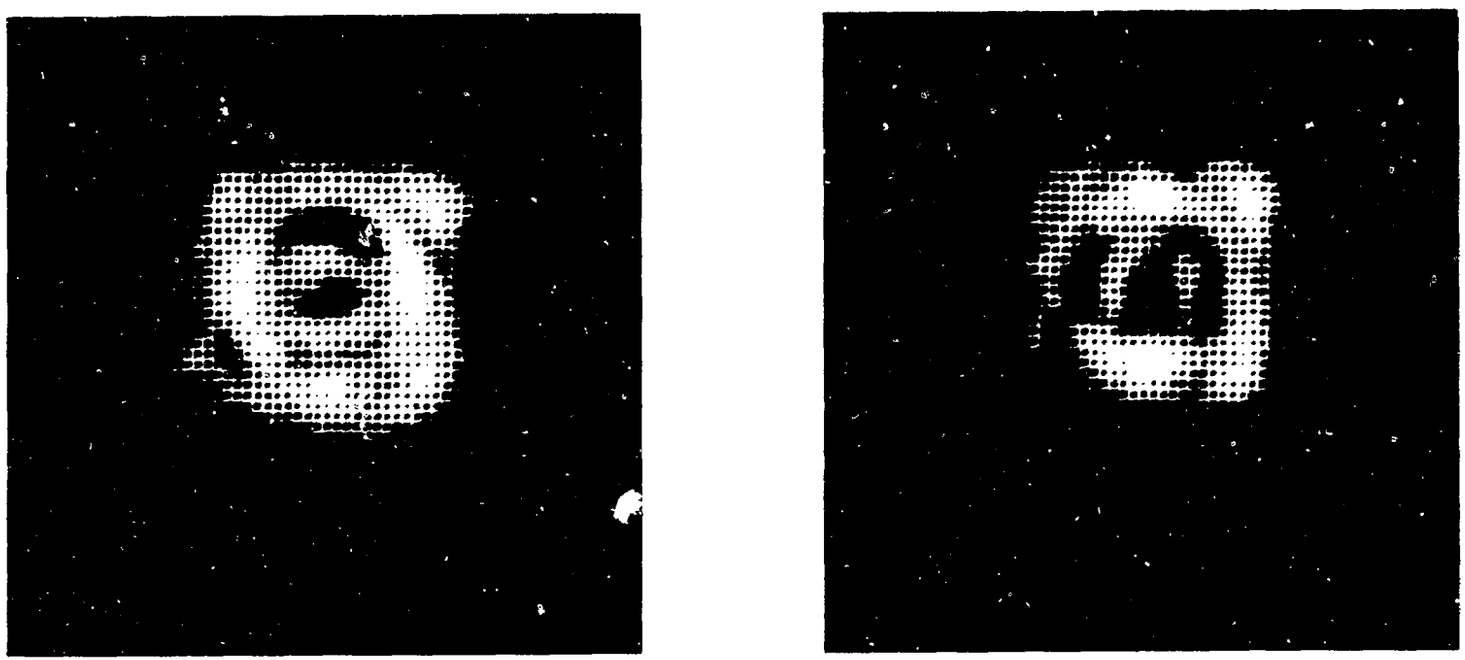

a) E-polarized

b) H-polarized

Figure 5-6. Images of Object C in IV with two Polarizations at γ Hz

6. REFLECTION VECTOR LOCUS PLOTS

The ability of the microwave imaging system to identify buried objects has clearly been demonstrated, but the high resolution is obtained at the expense of limited field of view; this trade-off problem is common to all imaging systems: telescopes, microscopes, etc. The amount of data that can be processed is constrained by the computer size (cost) and the time on range available for calculation. Moreover, the complexity of the surface fitting procedure for reducing background noise increases with field of view and becomes impossible for vast areas. Therefore, to use the imaging system efficiently, the location of the buried objects must first be determined to within a small area, 3' x 3' for example. In this section, we shall describe one detection technique that uses the same equipments as the imaging system.

A reflection vector locus (RVL) plot traces the history of the received signal in the complex plane as the antenna scans over a surface. When the received signal consists of the front surface reflection alone, the RVL would cluster around a single point for level surfaces and a curved line for moderately sloping surfaces; examples were shown in Figures 4-1 and 4-2. When the antenna scans over a buried object, the total object scattered field adds to the surface reflection vectorially, and gives a different RVL. Figures 6-1 and 6-2 show two scans each over object B in Sector III and object C in Sector IV respectively, using the NBS data taken at αHz.

The scattering cross-section of object B is small so that the object field behaves essentially like a single component and as it changes amplitude and phase the RVL spirals out and forms a figure eight. The RVL's of object C are noticeably more complicated. The reason is that while for object B there is a single vector added to the surface reflection (Figure 6-3a), the scattered field of object C consists of several components due to the complex structure, each moving in its own way (Figure 6-3b). As the object depth increases, the RVL becomes smaller but still maintains its shape, until the object scattered field is masked by the variation in the surface reflection component.

Therefore, one way to detect buried objects is to display these RVL's continuously as the antenna scans over a surface of interest. When the operator observes some unusual deviations in the RVL he can move the antenna back and form a hologram for imaging. As shown in Figures 6-1 and 6-2 each object has its own characteristic RVL, like a signature. For a finite number of interesting objects, an operator can be trained to identify them by simply looking at the RVL's, although the probability of misses would be smaller if he can look at the images also.

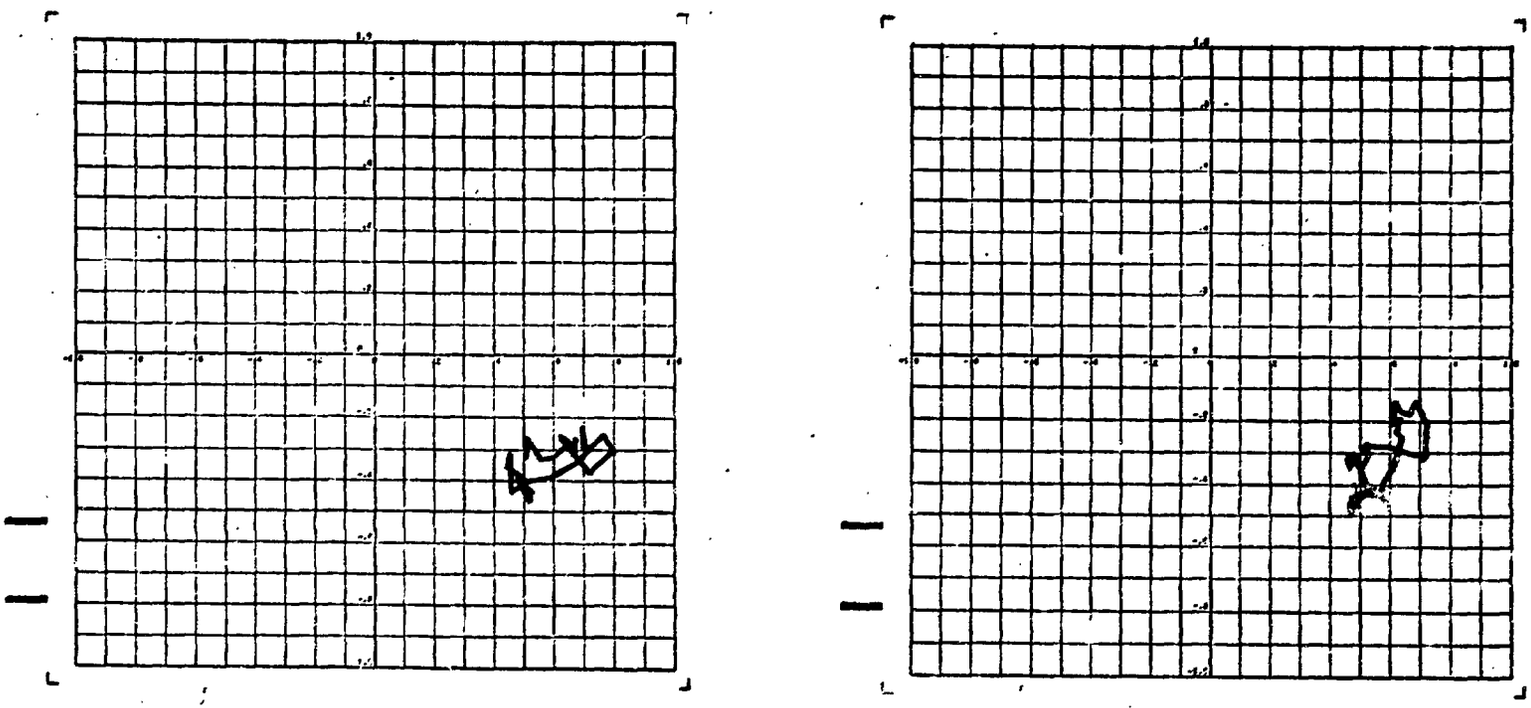

Figure 6-1. Reflection Vector Loci of Object B in III at α Hz.

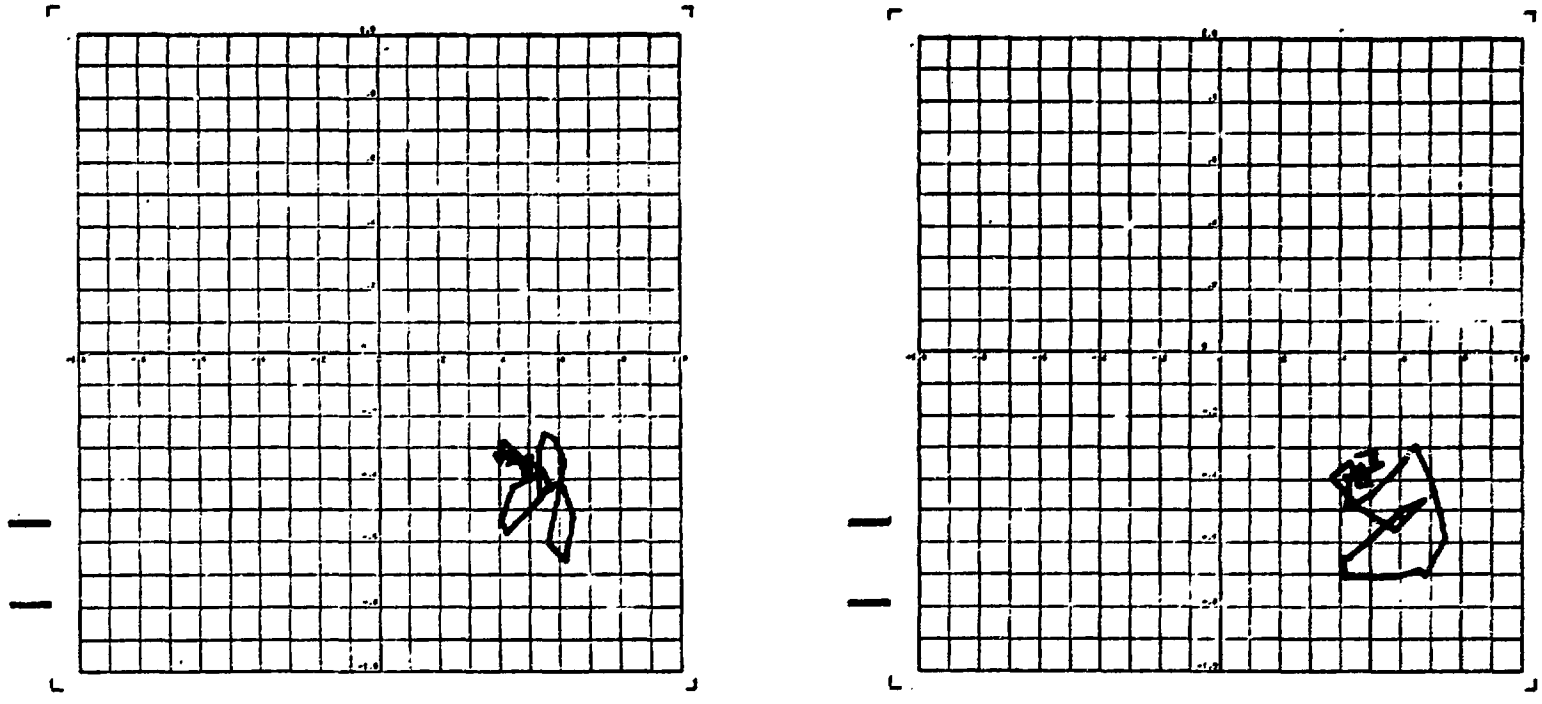

Figure 6-2. Reflection Vector Loci of Object C in IV at α Hz.

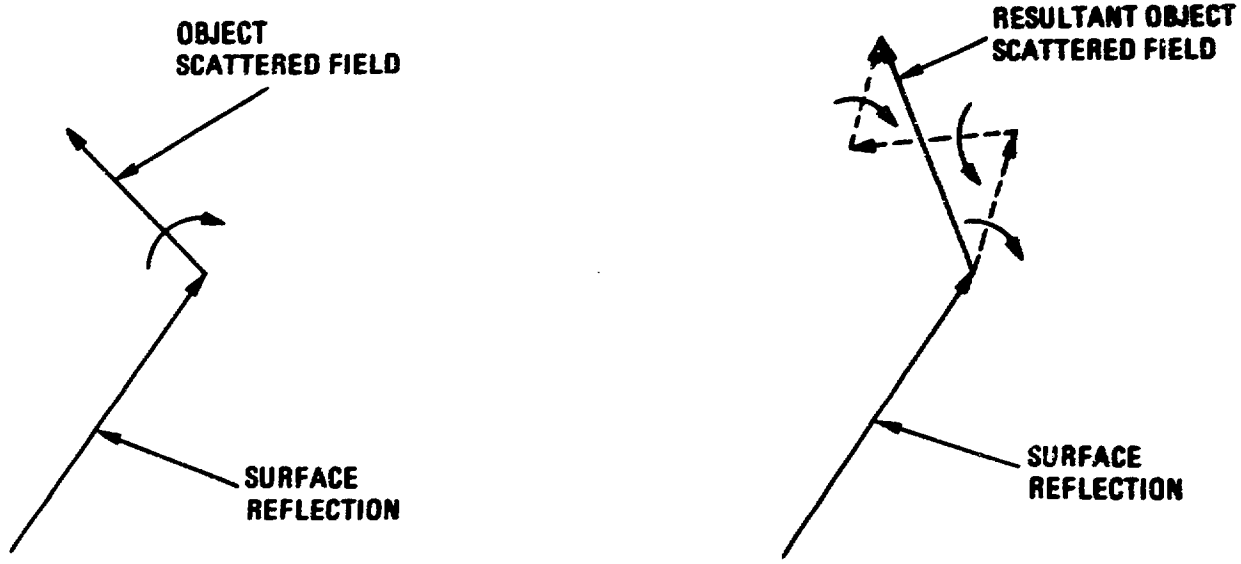

a) Object B

b) Object C

Figure 6-3. Components in Reflection Vector of Objects B and C

7. CONCLUSION

The program demonstrated the feasibility of imaging buried dielectric objects under conditions that were more realistic than those utilized in an earlier feasibility demonstration, which was described in Reference 1. Specifically, realistic objects were utilized, the soil surface was rough, and the soil was damp. In the first demonstration only one object had been used and that was in smooth dry soil.

The parameters considered in the program were the object configuration and its buried depth, soil moisture and surface roughness, as well as the frequency and polarization of the microwave energy that was utilized for measurements. Images were successfully formed for all three objects utilized. Image quality depended on all the parameters mentioned above.

Phase and intensity were measured with a continuous wave system and a monostatic antenna that scanned an area to synthesize a hologram, and the measured data were computer processed to form images. The successful image formation verifies the validity of an approximate algorithm, which is based on the angular spectrum concept and backward propagation. The same propagator had previously been tested for smooth, dry soil. The propagator function approximates the effect of the air-soil interface and the difference in propagation wavelength in the soil. This approximation is practical because the soil constitutive parameters are generally unknown.

The program verified the feasibility of subtracting the field reflected by the air-soil interface from the total field. The front surface reflection is noise, and the signal is the field reflected from the object. In fact, in some cases the object can be recognized from the data following subtraction, but without inverse propagation. The reason is that the measurements are made in the nearfield of the object so that diffraction spreading is negligible.

In general, for the NBS data the images of objects A and C were better than those of object B. This conclusion indicates that object B has dielectric constant that more nearly matches that of the soil and that the internal inhomogeneities are smaller. Images of object A were formed for both depths that were utilized, and images of object C were formed for all three depths utilized. For object C at one of the two frequencies utilized image quality was best for a depth midway between the deepest and shallowest utilized; however, for another frequency, the shallowest depth gave the best image. Object B was difficult to image but images were formed of its small void region.

Images were also made with data measured at GD/E with very dry, very smooth soil. These images were standard for comparing with the images for rough, damp soil. Image quality was better than that for the damp soil, rough surface at NBS . For object C considerable structural detail was present in the images, and correlated with the object's structure. Improved images of object B were also obtained. Image features present in the standard images were present in the images for rough, damp soil but the noise was greater for the rough, damp soil.

To summarize, this report again demonstrates the feasibility of microwave imaging buried object. The results are technical justification for additional development, specifically of a more automated system with an array of antennas and of additional measurements on rough surfaces.